Supplemental Information

Hippocampal Network Dynamics

during Rearing Episodes

Albert M. Barth, Andor Domonkos, Antonio Fernandez-Ruiz, Tamas F. Freund, and Viktor Varga
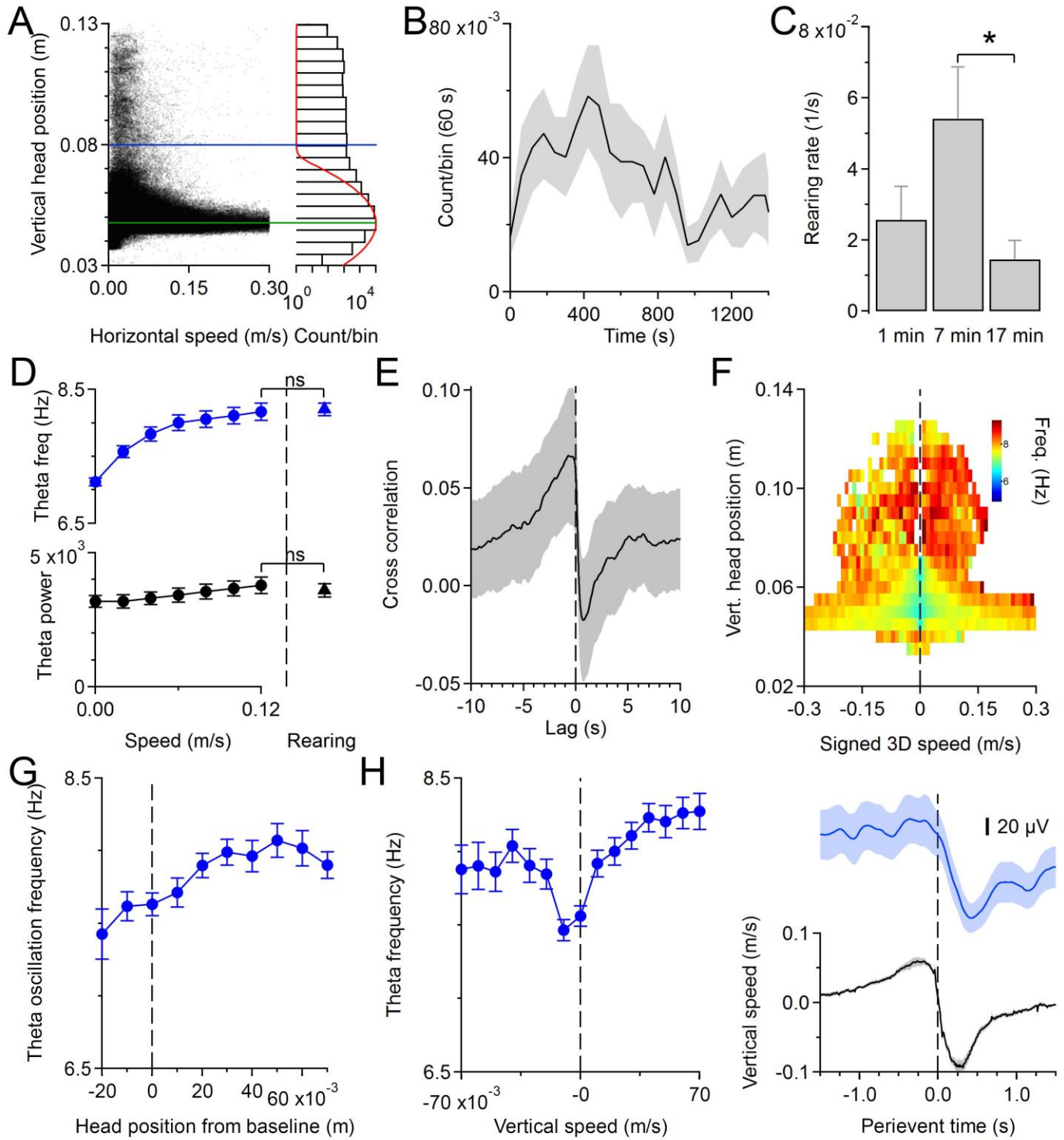
Supplemental figures

Figure S1. Rearing events, related to figure 1. A) Detection of rearing events. Left: vertical head position plotted against horizontal running speed. Right: corresponding histogram of the vertical head positions. Red trace shows the fitted Gaussian curve (see Methods). Green line indicates the peak of the Gaussian curve, blue line denotes the threshold for rearing event detection. B) Time evolution of rearing incidence in open field (mean ± s.e.m, average n=12 animals). C) Rearing incidence reaches maximum around 7 min in open field (* $p<0.05$, n=12 animals, ANOVA with post-hoc Tukey HSD). D) Theta oscillation frequency and power increased with running speed but it was not significantly different from that is observed during rearing episodes ($p>0.05$, n=12 animals, paired t-test). E) Average cross-correlogram of the vertical head position vs high (7-12 Hz) theta oscillation power (mean ± s.e.m, n=12 animals). F) 3D speed-vertical head position 2D histogram from a representative animal. We rendered + or – sign to the 3D speed depending whether the head moved up- or downward. Note that higher theta frequencies appeared at higher 3D speeds at lower head positions and at lower upward 3D speeds at higher head positions. G) Summarized data of theta oscillation frequency as a function of vertical head position (Pearson's $r = 0.32$, $p=0.002$, n=12 animals). Note the flattening of the curve at higher head positions. Zero vertical head position indicates the baseline value (see: Supplemental Experimental Procedures). H) Summarized data show theta oscillation frequency depending on vertical head speed (*left*). Note the prominent dependence of theta oscillation frequency on upward vertical speed (Pearson's r for negative/downward speeds: -0.28, $p=0.005$, for positive/upward speeds: 0.51, $p=1.1x10-7$, n=12 mice). Vertical head speed starts to decrease before rearing peaks (*right bottom, black trace,* mean ± s.e.m, average n=12 animals) and the corresponding high theta magnitude also shows a decreasing tendency before rearing peak (*right top, blue trace,* mean ± s.e.m, average n=12 animals).
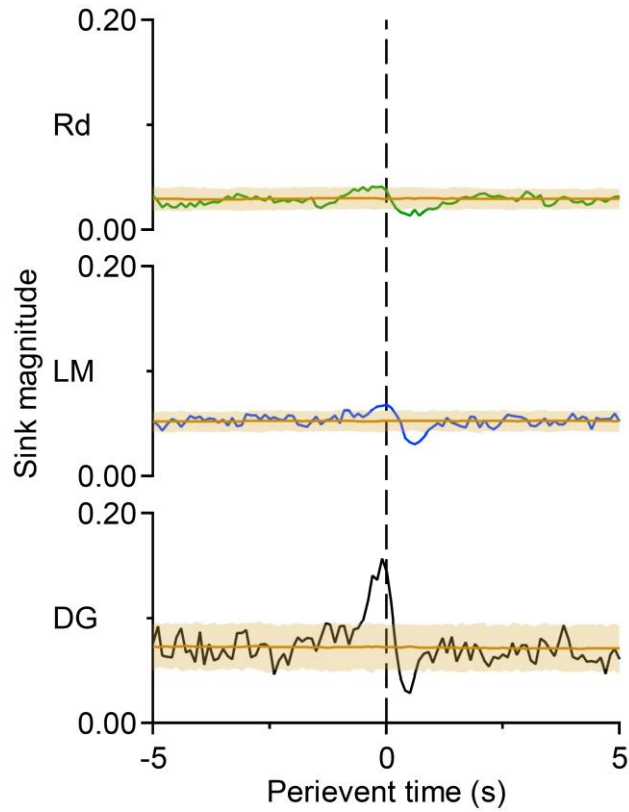
Figure S2. Perievent sink magnitude, related to figure 2. Rearing peak triggered magnitude of the 3 main sinks. Note the robust enhancement of the dentate sink. Brown traces indicate the shuffled control, shaded area represents the 99 % band of the shuffled control (*n=5* animals). Rd: radiatum, LM: lacunosum-moleculare, DG: dentate gyrus sinks.
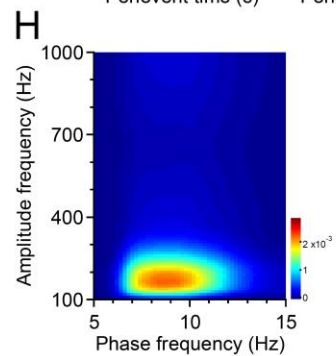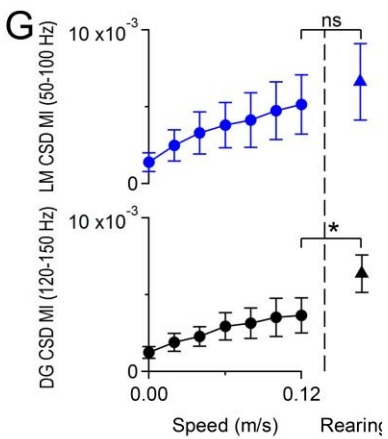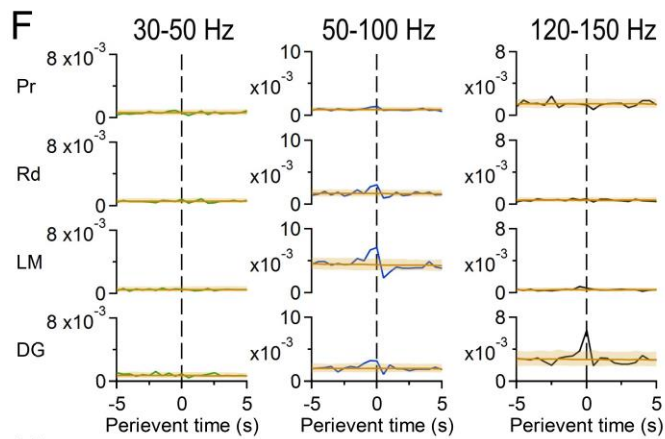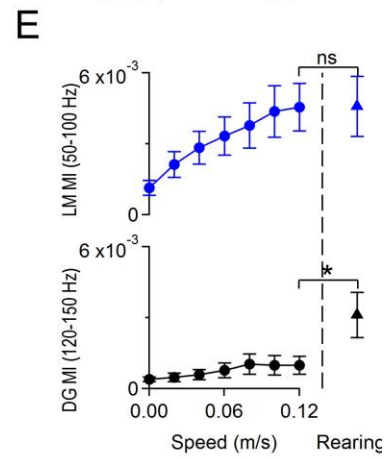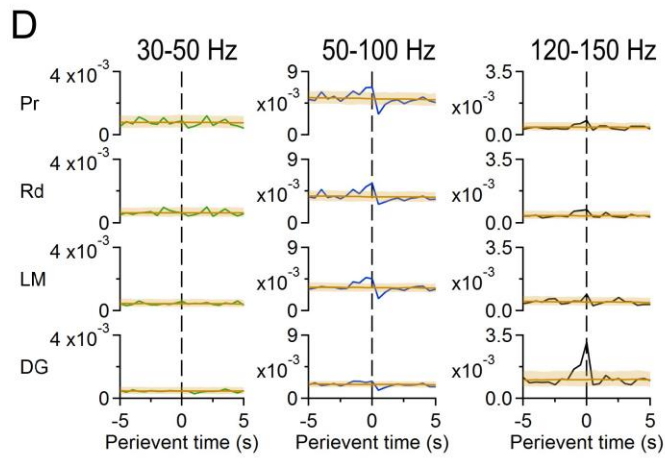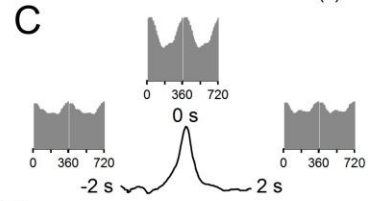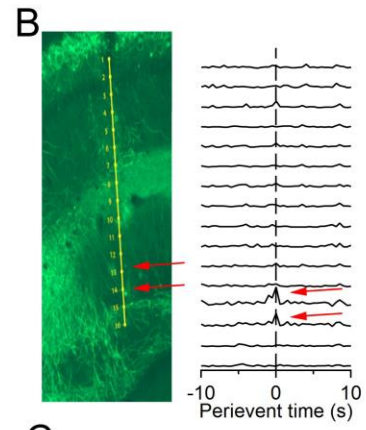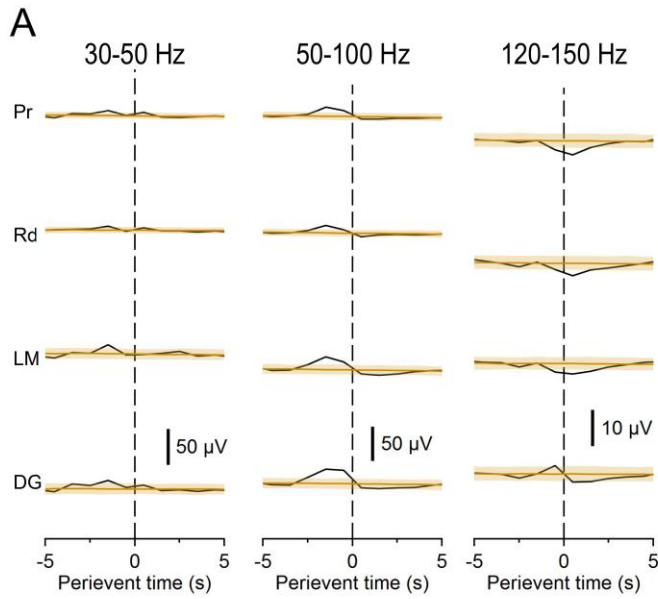
Figure S3. Gamma activity during rearing, related to figure 3. A) Average binned (bin size 1 s) rearing peak triggered perievent power in 3 different frequency bands and in different layers of the hippocampal formation. Note the tendency for mid and fast gamma increment around rearing peak. However, the layer specificity is distorted by volume conduction (brown traces indicate the shuffled control, shaded area represents the 99 % band of the shuffled control, $n=7$ animals). B) Sample perievent theta-gamma coupling values for fast gamma (120-150 Hz) at different depth of the hippocampal formation. Arrows indicate the robust enhancement of theta-gamma coupling around the rearing peak in the dentate gyrus. C) Sample theta-fast gamma phase amplitude histograms at 3 different time points around rearing peak. Black trace indicates vertical head position. D) Average perievent theta-gamma coupling values in 3 frequency bands and in the main layers of the hippocampal formation calculated from Hilbert magnitude values (brown traces indicate the shuffled control, shaded area represents the 99 % band of the shuffled control, $n=7$ animals). Note the prominent increment of theta-coupled fast gamma in the dentate gyrus. The mid gamma layer specificity is distorted by the presence of volume conduction. E) The coupling of LM mid gamma but not dentate fast gamma to theta oscillation increases with running speed (modulation index – running speed correlation Pearson's r for LM mid gamma: r=0.77, p<0.001; for dentate fast gamma: r=0.26, p > 0.1). However, rearing-coupled dentate theta – gamma coupling values were about 2 times as large as what was observed during running (* p<0.05, $n=7$ animals, paired t-test). F) Average perievent theta-gamma coupling values in 3 frequency bands and in the main layers of the hippocampal formation calculated from CSD traces (brown traces indicate the shuffled control, shaded area represents the 99 % band of the shuffled control, $n=5$ animals). G) The coupling of LM mid gamma and dentate fast gamma to theta oscillation increases with running speed calculated from CSD traces (modulation index – running speed correlation Pearson's r for LM mid gamma: r=0.61, p=0.001; for dentate fast gamma: r=0.46, p = 0.02). Note that dentate theta-fast gamma coupling values were about 2 times larger than that during running (* p<0.05, $n=5$ animals, paired t-test). H) Average crossfrequency-amplitude comodulogram for dentate gyrus LFP recordings. Note the restricted appearance of the theta dentate fast gamma coupling and the lack of CFC at higher, multiunit-contaminated frequencies (averages of $n=5$ animals). For A, D, F: Pr: pyramidal layer, Rd: radiatum, LM: lacunosum-moleculare, DG: dentate gyrus.
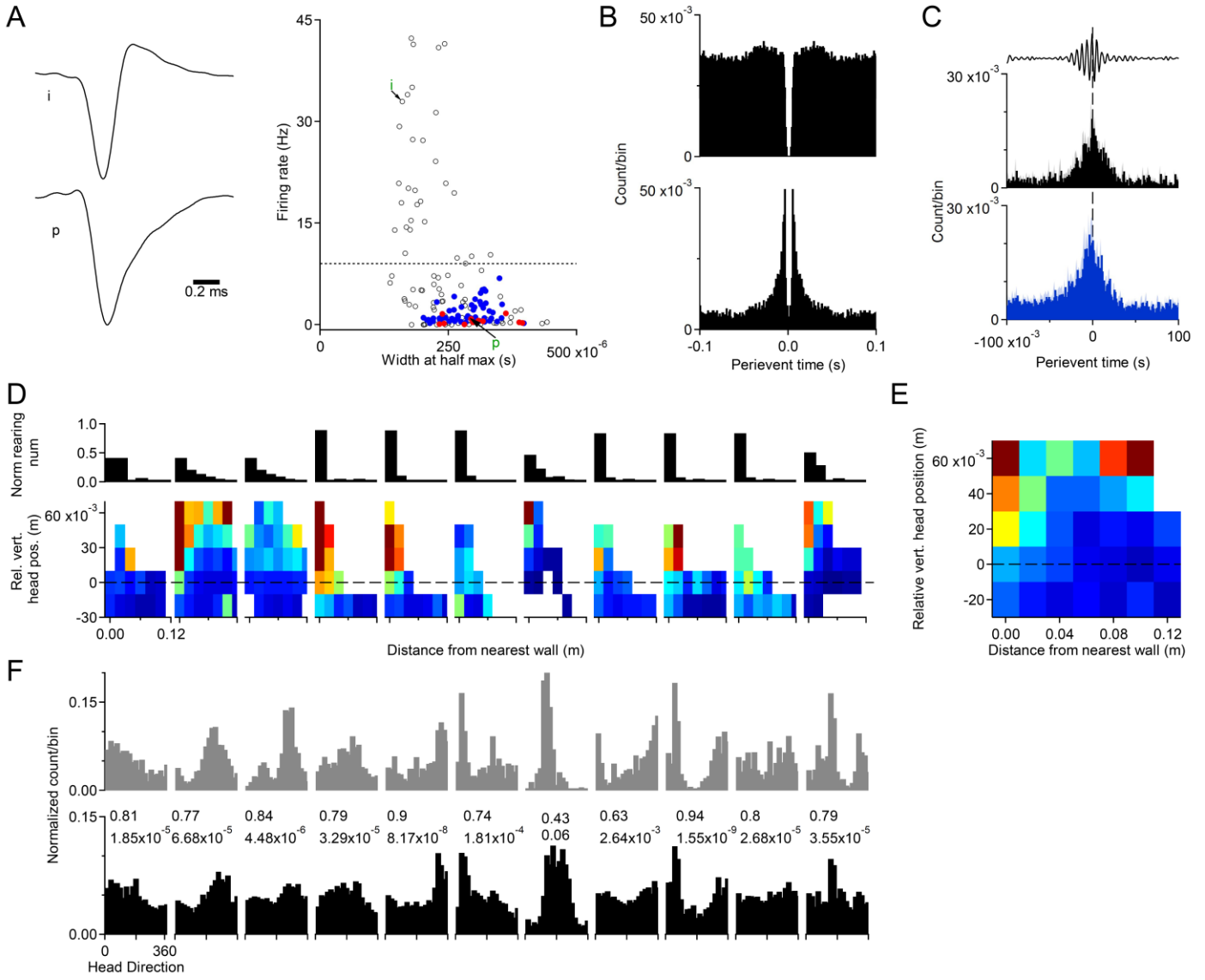
Figure S4. Basic characteristics of separated units, related to figure 4. A) Sample putative interneuron (left top, i) and principal (left bottom, p) cell average waveforms registered in the CA1 pyramidal layer. Single units could be best separated based on their firing rate (right). Blue filled circles: place cells, red filled circles: rearing-ON units. Horizontal dashed line indicates the border between putative pyramidal and interneurons. Green "i" and "p" indicate the sample units on the left side. B) Autocorrelograms of a putative interneuron (*top*) and principal (*bottom*) cell (bin size = 1 ms). Cells are the same as in A. C) Rearing-ON units and place cells show increased activity during sharp wave ripples. Sample 150-250 Hz filtered LFP trace showing a sample ripple (top). Average ripple peak-triggered perievent histogram of rearing-ON units (middle, *n=6* units). Note that for the remaining 5 rearing-ON units there were not enough number of ripple events during the recording period. Average ripple peak-triggered perievent histogram of place cells (bottom, *n=12* units). D) 2D histograms present the border and vertical head position firing preference of rearing-ON units (*bottom*), above is the corresponding distribution of all rearing events from the nearest wall (*top*). Horizontal dashed line on the bottom diagrams indicates the threshold for rearing events. E) Average wall distance-vertical head position 2D histogram of the rearing-ON units (*n=11*). In D and E red-brown colors indicate higher normalized spike numbers. F) Head direction tuning of rearing-ON units. Histograms in grey present the observed head direction tuning of the rearing-ON units (*top*), below the corresponding horizontal position-based reconstructed (see Supplemental Experimental Procedures) tuning histograms (*bottom*, black histograms). Numbers in the middle indicate the corresponding Pearson's r (upper number) with the p value (lower number). Note the high correlation values between the observed and reconstructed tuning curves.

Table S1 related to figure 1. Summary table presenting details about the 12 mice involved in this study.

Animal ID	Genotype (C57Bl/6J)	Number of trials	Previous experience (min)	Dorsal hippocampus probe (NeuroNexus)	Number of rearing events	Analysis of spectral changes in low frequency bands	Analysis of LFP theta-gamma coupling	Analysis CSD	Analysis ICA	Analysis units
1957	Vgat-ires-Cre	1	33	A1x32-6/10mm-50-177	132	yes	yes	yes	yes	
1959	Vglut3-ires-Cre	1	0	Buzsaki32	74	yes				
1966	Som-ires-Cre	1	40	A1x32-6/10mm-50-177	45	yes	yes			
1969	Som-ires-Cre	1	0	A1x32-6/10mm-50-177	29	yes	yes			yes
1971	Som-ires-Cre	1	0	Buzsaki32	38	yes				yes
1977	Som-ires-Cre	1	45	A1x32-6/10mm-50-177	65	yes	yes	yes	yes	
1982	Som-ires-Cre	1	30	A4x16-6mm-50-703, A1x32-6/10mm-50-177	27	yes	yes	yes	yes	yes
1984	wild type	1	0	A1x16-6/10mm-100-177	84	yes	yes		yes	yes
1986	Som-ires-Cre	1	11	A4x16-6mm-50-703, A1x32-6/10mm-50-177	17	yes	yes	yes	yes	yes
1989	Som-ires-Cre	1	0	Buzsaki32	19	yes				yes
1991	Vglut3-ires-Cre	1	0	Buzsaki32	74	yes				yes
2089	wild type	3	0	A1x64-Poly2-6mm-23s-160	176	yes				yes

Only animals implanted with linear type silicone probes could be used for CSD and ICA analysis. In one animal the linear probe was located at the apex of the dentate gyrus, in two other animals there were several bad channels on the linear probe thus, recordings from these animals could not be used for reconstructing the CSD and ICA. In one other animal the linear probe was just above the granule cell layer therefore it could not be used for dentate CSD map analysis. Under the "previous experience" (4.) column we summarized the time each animal spent in the same arena within 5 days preceding the recordings.

Supplemental experimental procedures

CONTACT FOR REAGENT AND RESOURCE SHARING

Further information and requests for resources and reagents should be directed to and will be fulfilled by the Lead Contact, Viktor Varga (varga.viktor@koki.mta.hu).

RESOURCE TABLE

REAGENT or RESOURCE	SOURCE	IDENTIFIER
Experimental Models: Organisms/Strains		
Mice: C57Bl/6JCrl wild type	Inst. Exp. Med. own animal facility	N/A
Mice: vGLUT3-ires-Cre	The Jackson Laboratory	https://www.jax.org/strain/018147
Mice: SOM-ires-Cre	The Jackson Laboratory	https://www.jax.org/strain/013044
Mice: vGAT-ires-cre	The Jackson Laboratory	https://www.jax.org/strain/016962
Software and Algorithms		
MATLAB	MathWorks	**RRID:SCR_001622**
SpikeDetekt	Rossant et al., 2016	https://github.com/klusta-team/spikedetekt
KlustaKwik	Rossant et al., 2016	**RRID:SCR_014480**
KlustaViewa	Rossant et al., 2016	https://github.com/klusta-team/klustaviewa/)
Spyking Circus	Yger et al., 2016	https://github.com/spyking-circus/spyking-circus
Phy	http://phy-contrib.readthedocs.io/en/latest/template-gui/	https://github.com/kwikteam/phy
ICA algorithms	EEGLAB	https://sccn.ucsd.edu/eeglab/
Igor Pro7	Wavemetrics Inc	**RRID:SCR_000325**
OptiTrack	NaturalPoint Inc	http://optitrack.com/software/
Other		
Silicone probe: 32-sites, 4-shank probe	NeuroNexus	Buzsaki32
Silicone probe: 32-sites, 1-shank probe	NeuroNexus	A1x32-6mm-50-177
Silicone probe: 64-sites, 4-shank probe	NeuroNexus	A4x16-5mm-50-500-703
Silicone probe: 64-sites, 1-shank probe	NeuroNexus	A1x64-Poly2-6mm-23s-160
256 channel Multiplexed Biosignal Amplifier	Amplipex	http://www.amplipex.com/products/large-scalerecording/?single_prod_id=37

METHODS DETAILS

Animal surgery

Animals were anesthetized with isoflurane anesthesia and mounted in the stereotaxic frame (David Kopf Instruments, Tujunga, CA). The cranium was exposed and one or several craniotomies were performed under stereotaxic guidance. Linear or Buzsaki32 type silicon probes (Table S1, NeuroNexus, Ann-Arbor, MI) were implanted in the dorsal hippocampus. The probes were fixed on custom-made micro-drives attached to the skull with dental acrylate. The craniotomies were sealed with artificial dura (Cambridge NeuroTech Ltd, Cambridge, UK). Two stainless steel screws placed above the cerebellum served as ground and reference for the recordings.

The probe-microdrive ensemble was shielded by a copper mesh preventing the contamination of the recordings by environmental electric noise. Following the surgery, the animals were continuously monitored until recovered as demonstrated by their ability to exhibit purposeful movement. After post-surgery recovery, the probes were moved gradually by the custom-made microdrive in 75 to 150 μm steps per day until the target area was reached.

The pyramidal layer in the CA1 region was identified physiologically by increased unit activity and the occurrence of ripple activity. The identification of CA1 and dentate gyrus layers was achieved by the application of current source density and independent component analysis to the local field potentials (Fernández-Ruiz and Herreras, 2013; Fernández-Ruiz et al., 2012) and by characteristic physiological markers such as the reversal of sharp-waves and depth profile of theta oscillation amplitude.

Data acquisition

Animals were placed in a rectangular arena (60 x 60 cm, 20 cm wall height) to allow spontaneous open field exploratory behavior. The arena walls and floor were made of grey plastic. Specific extra-box cues were not used, however from the arena the animals could see the experimental room. Some animals used in this study already had previous experience in the same arena within 5 days before recordings (see Table S1).

Electrophysiological recordings were performed by connecting the implanted silicone probe to a signal multiplexing headstage attached to a flexible lightweight cable. Electrophysiological signals were acquired at 20k sample/s (KJE-1001, Amplipex Ltd, Hungary).

The movement of the animal was tracked by an infrared marker-based high speed (120 frame / sec) 4-camera (Flex13, NaturalPoint, Inc., Corvallis, OR) motion capture system capable of reconstructing the animal's position and orientation in 3 dimensions with submillimeter resolution (Motive, OptiTrack, NaturalPoint, Inc., Corvallis, OR). The infrared-reflective markers (3 mm diameter hemispheres) were attached to the head-assembly of the mice or to the headstage.

Tissue processing

Following the termination of the experiments, animals were deeply anesthetized and transcardially perfused first with 0.9% saline solution followed by 4% paraformaldehyde solution. Brains were sectioned in 60-μm thick slices (Leica Biosystems, Wetzlar, DE). Probe tracks were reconstructed on the consecutive tissue slices.

Detection of rearing events

A histogram of all sampled vertical head positions was generated and a Gaussian was fitted to the left part of the histogram not skewed by rearing events. The mean of the fitted Gaussian was considered to be the mean baseline head position. Vertical headposition bin where the fitted Gaussian returned to 0 was defined as rearing threshold (Figure S1A).

Validation of rearing definition

To validate our rearing definition, we carried out further experiments to investigate the forelimb position relative to the ground and the vertical head position. We glued a mock head assembly with infrared markers and headstage connectors to the head of 3 mice, but without implanting electrodes. From the three mice one exhibited enough rearing events. The size and shape of the „dummy" headmounts were similar to those with electrodes used in this study. The camera configuration of the 3D tracking system was modified: one of the four top mounted cameras was placed at the ground level of the open field arena to provide side view of the animal. The wall of the arena in front of the side camera was removed. By elevating the floor, we created a 5 cm drop to prevent escape from the arena. The height of the sideview camera was adjusted to show the horizontal line of the ground plane. During tracking we connected the animal to the cable the same way as during electrophysiological recordings but only tracking data was registered. Tracking data and sideview video were offline analyzed. The videos were manually analyzed by looking for frames corresponding to the moment when both paws detached from the arena floor. We paired these frames with the tracking data to find vertical head positions corresponding to the release of the floor. Vertical head positions were measured relative to the mean baseline head position. We found that the vertical head position at the moment of paw detachment is, on average 34.8 ± 3.0 mm. This value is very close to the average rearing threshold used in this study: 34.4 ± 2.6 mm.

Time-frequency analysis

To analyze oscillatory activity during rearing events we obtained the Morlet wavelet decomposition or Hilbert transformation of the LFP recordings. The Hilbert magnitudes of different frequency bands were averaged by triggering on rearing peaks. Shuffled averages were generated for each frequency band by randomly selecting timepoints in the 20 s interval (10 s before, 10 s after) around each rearing peak repeated by 1000 times. The perievent average traces were plotted with the corresponding 99% confidence bounds of the shuffled data. If the average trace exceeded the 99% confidence bounds at least for 0.5 s (> 5% of rearing event duration) during rearing event, we defined as significant alterations. We further verified the significance of the alterations by comparing values during rearing and baseline periods (5-10 s before rearing peak). We performed the above shuffling procedure, and applied the same criteria of significance for perievent modulation indices calculations (see Figure 3H and Figure S3D,F).

We defined the onset of the significant alteration (for Figure H) when the perievent average trace crossed the 95 % confidence bound of the shuffled control for at least 0.2 s.

Cross-correlation analysis

Time lag between change of vertical head position and alteration of power in the high theta band was calculated from their cross-correlogram (CCG). First, both time series were downsampled to 100 Hz and their mean was subtracted. Then, the CCG was computed by Igor Pro's built-in cross-correlation function. The time of the CCG's positive peak corresponded to the time lag between the two time series.

Current source density analysis

To produce current source density (CSD) estimates the second spatial derivatives of the voltage profile were calculated (Nicholson and Freeman, 1975). To calculate CSD during rearing the second spatial derivatives were averaged around theta cycle peaks closest to rearing peaks. For CSD analysis during running episodes, segments when movement speed was above 4 cm/s were used.

Independent Component Analysis of LFPs

To address the inverse problem of LFPs, that is, to separate the different sources that contribute to the mixed signal, we employed a combination of independent component analysis (ICA) and current source density (CSD) analysis as had been described and validated previously (Fernández-Ruiz and Herreras, 2013; Fernández-Ruiz et al., 2012).

ICA is a blind source-separation technique (Bell and Sejnowski, 1995; Comon, 1994) that can isolate spatially segregated stable patterns of activity in a mixed signal recorded with an array of sensors. Applied to linear profiles of LFPs it can separate physiologically meaningful sources that can be attributed to known anatomical pathways, as has been demonstrated for the CA1, CA3 and dentate regions of the rat hippocampus (Benito et al., 2014; Fernández-Ruiz and Herreras, 2013; Fernández-Ruiz et al., 2012).

Here, we applied ICA to spatially contiguous LFP channels along the dorso-ventral hippocampal axis. The algorithm takes a time series of data with dimension equal to the number of recording sites, and returns a time series of the same dimensionality, but rotated such at each dimension to represent a different IC. The inverse of the mixing matrix that transforms the LFP data into the ICs gives the channel weight of each component that is captured for each electrode. When plotted according to the anatomical location of the electrodes, this corresponds to the spatial voltage loadings of each IC (Fernández-Ruiz et al., 2012). Once ICs have been extracted from the raw LFP traces, they can be analyzed as if they were active independently from activities at other locations.

The optimization of ICA of LFPs for high-frequency activity require a series of pre-processing steps that have been described in detail elsewhere (Fernández-Ruiz et al., 2017; Schomburg et al., 2014).

Cross-Frequency Coupling of LFPs

Theta-band phase of the LFP recorded in CA1 pyramidal layer was calculated by Hilbert transformation of the 5-12 Hz bandpass filtered LFP. Theta epochs were detected where the animals' running speed exceeded 4 cm/s for 2 s. Theta peaks correspond to 180° and troughs to 0° and 360° of theta waves recorded in the CA1 pyramidal layer throughout the manuscript.

To analyze high-frequency oscillatory activity in the LFP at a high resolution in time and frequency, the continuous wavelet transform (CWT) of the LFP (or ICs) was calculated using complex Morlet wavelets (Torrence and Compo,

1998). The phase-amplitude cross-frequency coupling (CFC) during theta oscillations for a given LFP recording was assessed using the modulation index (MI) (Tort et al., 2010). Wavelet phase was calculated at 100 levels from 0.2-20 Hz, and the amplitude at 170 levels from 30-200 Hz. Phase time-series were binned into phase intervals and the mean wavelet amplitude was calculated for each of them (Fernández-Ruiz et al., 2017). The MI was obtained by measuring the divergence of the observed amplitude distribution from the uniform distribution. The statistical significance of the MI values was assessed by a surrogate analysis (n = 500 surrogates) with random shifts between the phase and amplitude time series (Canolty et al., 2006).

All LFP analysis was performed with custom-made MATLAB (The MathWorks, Inc., Natick, MA) and IgorPro7 (Wavemetrics, Lake Oswego, OR) scripts available upon request.

Spike sorting

Neuronal spikes were detected and automatically sorted from the high-pass filtered LFP (0.5–5 kHz) either by the masked EM or by a template matching algorithm (KlustaKwik (Rossant et al., 2016) or Spyking-Circus (Yger et al., 2016) followed by manual adjustment of the clusters using the KlustaViewa or Phy softwares (Rossant et al., 2016) to obtain well-isolated single units. Cluster isolation quality was estimated by calculating the interspike interval index for each cluster (Schmitzer-Torbert et al., 2005); poor quality clusters were discarded.

Putative pyramidal cells and interneurons were separated on the basis of their firing rate, spike width and autocorrelograms (Csicsvari et al., 1998).

Definition of rearing-ON units and place cells

All place cells and rearing-ON units were identified as putative principal units in the CA1 pyramidal layer of the dorsal hippocampus. The rearing-ON units were defined based on their rearing peak triggered perievent histograms. Shuffled control perievent histograms were created based on randomly selecting timepoints within a 20 s window of each rearing event. The observed and shuffled control perievent histograms were compared (Wilcoxon-Mann-Whitney-test) and if there were significant firing increment around rearing peaks (-0.25 and +0.25 s) the unit was defined as rearing-ON units. Place cells were defined based on their 2D firing rate map. The arena was divided into 2 x 2 cm spatial bins. The dwell time normalized firing rate was calculated in each spatial bin. Place field was defined as at least 5 continuous spatial bins where the firing rates were above the mean firing rate + at least 2 standard deviations. A place cell was defined if it had at least one place field and the corresponding spatial information was above 0.5. Rate map, spatial information and sparsity were calculated as previously described (Skaggs et al., 1996). Place fields with fewer than 50 spikes were discarded.

Activity of rearing-ON units

The average rearing peak-triggered perievent histogram of rearing-ON units indicate robust enhancement around rearing peaks. However, rearing-ON units show elevated activity only in a subset of rearing events ("active" rearing events for that rearing-ON units). A baseline firing rate was calculated 5 – 10 s before each rearing peak and active rearing events

were defined when the firing rate exceeded the baseline firing rate with 1 standard deviation in a 1 s window around the rearing peak.

We further investigated the spatial dispersion of these active rearing events for each rearing-ON unit (i.e. rearing events with associated ON unit activation, shortly active events). As a null hypothesis we assumed that the spatial dispersion of active events, namely the average distance between any two active events is equal to the distance of any two randomly selected rearing events (independent of their association with ON unit activation). To test against the null hypothesis first for each rearing-ON unit, rearing events were randomly selected to get an equal quantity to the number of active events. Then the average horizontal distance among the spatial location of the selected events was calculated and compared to the mean distance among active events. The random selection and the corresponding average distance calculation was repeated 100 times.

The spatial distribution of active events was further analyzed by calculating their distance from the walls and defining a distance threshold of 5 cm based on which all rearing episodes were divided into peripheral and central events and the proportion of active events in these categories was determined.

Reconstruction of head direction curves

To investigate the head direction tuning of rearing-ON units it is important to analyze the effect of behavioral constrains which can result in apparent head direction tuning. The effect of behavioral constrains can be especially important at rearing related activity. We found that rearing events mostly occurred at the periphery where the animal preferentially faced toward the wall. To avoid this behavioral "bias" we followed previous reports to calculate reconstructed head direction tuning curves (Muller et al., 1994; Rubin et al., 2014). By comparing the observed and reconstructed head direction curves we tested whether head-direction tuning curves of the rearing-ON units could be a byproduct of the location of the firing locations.

DATA AND SOFTWARE AVAILABILITY

Data included and software used in this article will be available upon request.

Supplemental references

Bell, A.J., and Sejnowski, T.J. (1995). An information-maximization approach to blind separation and blind deconvolution. Neural Comput. *7*, 1129–1159.

Benito, N., Fernández-Ruiz, A., Makarov, V.A., Makarova, J., Korovaichuk, A., and Herreras, O. (2014). Spatial modules of coherent activity in pathway-specific lfps in the hippocampus reflect topology and different modes of presynaptic synchronization. Cereb. Cortex *24*, 1738–1752.

Canolty, R.T., Edwards, E., Dalal, S.S., Soltani, M., Nagarajan, S.S., Kirsch, H.E., Berger, M.S., Barbaro, N.M., and Knight, R.T. (2006). High gamma power is phase-locked to theta oscillations in human neocortex. Science *313*, 1626–1628.

Comon, P. (1994). Independent component analysis, A new concept? Signal Processing *36*, 287–314.

Csicsvari, J., Hirase, H., Czurko, A., and Buzsáki, G. (1998). Reliability and state dependence of pyramidal cell-interneuron synapses in the hippocampus: An ensemble approach in the behaving rat. Neuron *21*, 179–189.

Fernández-Ruiz, A., and Herreras, O. (2013). Identifying the synaptic origin of ongoing neuronal oscillations through spatial discrimination of electric fields. Front. Comput. Neurosci. *7*, 5.

Fernández-Ruiz, A., Makarov, V.A., and Herreras, O. (2012). Sustained increase of spontaneous input and spike transfer in the CA3-CA1 pathway following long-term potentiation in vivo. Front. Neural Circuits *6*, 71.

Fernández-Ruiz, A., Oliva, A., Nagy, G.A., Maurer, A.P., Berényi, A., and Buzsáki, G. (2017). Entorhinal-CA3 Dual-Input Control of Spike Timing in the Hippocampus by Theta-Gamma Coupling. Neuron *93*, 1213–1226.e5.

Muller, R.U., Bostock, E., Taube, J.S., and Kubie, J.L. (1994). On the directional firing properties of hippocampal place cells. J. Neurosci. *14*, 7235–7251.

Nicholson, C., and Freeman, J.A. (1975). Theory of current source-density analysis and determination of conductivity tensor for anuran cerebellum. J. Neurophysiol. *38*, 356–368.

Rossant, C., Kadir, S.N., Goodman, D.F.M., Schulman, J., Hunter, M.L.D., Saleem, A.B., Grosmark, A., Belluscio, M., Denfield, G.H., Ecker, A.S., et al. (2016). Spike sorting for large, dense electrode arrays. Nat. Neurosci. *19*, 634–641.

Rubin, A., Yartsev, M.M., and Ulanovsky, N. (2014). Encoding of Head Direction by Hippocampal Place Cells in Bats. J. Neurosci. *34*, 1067–1080.

Schmitzer-Torbert, N., Jackson, J., Henze, D., Harris, K., and Redish, A.D. (2005). Quantitative measures of cluster quality for use in extracellular recordings. Neuroscience *131*, 1–11.

Schomburg, E.W., Fernández-Ruiz, A., Mizuseki, K., Berényi, A., Anastassiou, C.A., Koch, C., and Buzsáki, G. (2014). Theta Phase Segregation of Input-Specific Gamma Patterns in Entorhinal-Hippocampal Networks. Neuron *84*, 470–485.

Skaggs, W.E., McNaughton, B.L., Wilson, M.A., and Barnes, C.A. (1996). Theta phase precession in hippocampal neuronal populations and the compression of temporal sequences. Hippocampus *6*, 149–172.

Torrence, C., and Compo, G.P. (1998). A Practical Guide to Wavelet Analysis. Bull. Am. Meteorol. Soc. *79*, 61–78.

Tort, A.B.L., Komorowski, R., Eichenbaum, H., and Kopell, N. (2010). Measuring Phase-Amplitude Coupling Between Neuronal Oscillations of Different Frequencies. J. Neurophysiol. *104*, 1195–1210.

Yger, P., Spampinato, G.L.B., and Esposito, E. (2016). Fast and accurate spike sorting in vitro and in vivo for up to thousands of electrodes. bioRxiv 1–21.